FAKULTÄT
FÜR !NFORMATIK
Faculty of Informatics

Noise Reduction in Medical DECT Data

BACHELORARBEIT

zur Erlangung des akademischen Grades

Bachelor of Science

im Rahmen des Studiums

Medieninformatik und Visual Computing

eingereicht von

Mirza Filipovic
Matrikelnummer 0225102

an der
Fakultät für Informatik der Technischen Universität Wien

Betreuung: Ao.Univ.Prof. Dipl.-Ing. Dr.techn. Eduard Gröller
Mitwirkung: Univ.Ass. Dipl.-Ing. Dr.techn. Gabriel Mistelbauer

Wien, 15.02.2014

(Unterschrift Verfasser) (Unterschrift Betreuer)

FAKULTÄT FÜR !NFORMATIK
Faculty of Informatics

Noise Reduction in Medical DECT Data

BACHELOR'S THESIS

submitted in partial fulfillment of the requirements for the degree of

Bachelor of Science

in

Media Informatics and Visual Computing

by

Mirza Filipovic
Registration Number 0225102

to the Faculty of Informatics
at the Vienna University of Technology

Advisor: Ao.Univ.Prof. Dipl.-Ing. Dr.techn. Eduard Gröller
Assistance: Univ.Ass. Dipl.-Ing. Dr.techn. Gabriel Mistelbauer

Vienna, 15.02.2014 ______________________ ______________________
(Signature of Author) (Signature of Advisor)

Erklärung zur Verfassung der Arbeit

Mirza Filipovic
Laudongasse 36/210, 1080 Wien

Hiermit erkläre ich, dass ich diese Arbeit selbständig verfasst habe, dass ich die verwendeten Quellen und Hilfsmittel vollständig angegeben habe und dass ich die Stellen der Arbeit – einschließlich Tabellen, Karten und Abbildungen –, die anderen Werken oder dem Internet im Wortlaut oder dem Sinn nach entnommen sind, auf jeden Fall unter Angabe der Quelle als Entlehnung kenntlich gemacht habe.

(Ort, Datum)	(Unterschrift Verfasser)

Kurzfassung

Im Bereich der medizinisch-diagnostischen Bildgebung hat die Dual Energy Computed Tomography (DECT) in letzter Zeit an Bedeutung gewonnen. Es wurde gezeigt wie durch DECT Messungen der Dichte und die Differenzierung zwischen Materialien verbessert werden können und dass die DECT-Bildgebung einen praktischen Gebrauch in der Medizin hat. Ein gebräuchliches Verfahren zur Verbesserung der Bildgebung stellt die Verringerung des Bildrauschens dar. In dieser Arbeit werden zwei Vorgehensweisen zur Reduzierung des Bildrauschens anhand von DECT Daten beschrieben. Als erstes wird gezeigt, dass der "cross/joint billateral filter" dazu verwendet werden kann um das Rauschen in DECT-Bildern zu verringern während gleichzeitig Kanten erhalten bleiben. Zweitens zeigen wir, dass das Rauschen in zwei DECT-Bildern antikorreliert ist und deshalb durch den Kalenders Correlated Noise Reduction Algoritmus effektiv entfernt werden kann. Weiters kann das Bildrauschen unter Berücksichtigung DECT spezifische Informationen, wie zum Beispiel die spektrale Informationen, zusätzlich reduziert werden. Ferner zeigen wir, dass die Effizienz des KCNR gesteigert werden kann, wenn zuvor die Korrektur der spektralen Informationen durchgeführt wurde [1]. Die AngioVis Software erlaubt die Darstellung und Bearbeitung von CT-Daten. Für die Umsetzung der Arbeit wurde ein Plugin im AngioVis Framework entwickelt.

Abstract

Dual energy computed tomography (DECT) recently gained popularity for medical diagnostic imaging. It has been demonstrated how DECT can improve density measurement and material differentiation, and practical applications for DECT imaging in medicine. Noise reduction is standard operation in the process of image enhancement which is necessary operation prior to image evaluation done by radiologist. In this work, we describe two approaches for noise reduction using DECT data. First, we show in the work that the cross or joint bilateral filter can be effectively used on DECT images to reduce noise while preserving edges. Second, noise in two DECT images is anti-correlated and can be effectively removed by the KCNR algorithm. Even better results can be achieved by using algorithms that exploit an additional characteristic information of DECT data, such as the spectral information. It was shown that the KCNR can increase its performance regarding quality when the spectral information is corrected before applying the KCNR [1]. AngioVis framework provides ability to present and manipulate CT data. All discussed image enhancement algorithms are implemented in AngioVis as a plugin.

Contents

CHAPTER 1

Introduction

Standard computed tomography (CT) provides single density data set of attenuation coefficients, whereas dual energy computed tomography (DECT) provide two separate data sets, which combined allow for more accurate density estimation and material differentiation. However, a superimposed data set from DECT exhibits a high level of noise. Hence, estimating the accurate density of a specific tissue is a difficult process, as described in the work of Park et al and Kalender et al. [1] [2]. The goal of this work is to implement, test and analyze algorithms in order to use advantages of both DECT data sets with the aim to reduce noise. These algorithms should preserve valuable details from both images, such as fine distinction between soft tissues of approximately the same density.

One very useful technique which is very well known from photography and which has the ability to preserve edges while removing noise is the so-called bilateral filter. The bilateral filter can be applied on CT data sets, and can be easily expanded to utilize benefits of DECT. The resulting data set is smoothed and noise is decreased, but at the same time edges are preserved. The bilateral filter does this task by considering spatial (neighboring densities) and range (density differences) domains, in the low energy and high energy images respectively, during filtering.

The attenuation of human tissue depends on the energy level used by the CT device and this information is useful for CT specific noise removal algorithms such as Kalenders correlated noise reduction (KCNR) [2] and spectral-error correction [1]. Depending on the applied energy level of the X-rays and depending on the tissue of interest, significantly different density values are acquired. These deviations from real world data are considered noise and errors.

CT errors in CT data sets are unfaithful representations of the scanned object. Examples of such errors are noise, beam hardening, Compton effect, motion artefacts, etc. Noise in the DECT data sets is correlated and can be successfully minimized with the KCNR algorithm, while preserving the quantitative information. The spectral-error is a specific type of CT error defined as the deviation from expected trends of material attenuation. The spectral-error can be detected using the fact that the attenuation of highly dense materials decreases more rapidly than the attenuation of materials with lower density, with increasing energy level of the CT scanner. To maximize the results of the spectral-error correction, two additional smaller corrections are performed beforehand, the water-offset correction and the zero-crossing pixels correction. The KCNR algorithm delivers a better noise reduction, if the spectral-error is corrected before, as stated by Park et al. [1].

We implemented our work in the AngioVis [3] framework as a plugin that provides a graphical user interface for setting parameters and performing the aforementioned correction operations. The bilateral filter can be used stand-alone or in combination with KCNR and spectral-error correction. The parameters of all operations can be adjusted to fit the needs of the desired medical examination.

The remainder of this work is organized as follows: Chapter 2 provides a brief overview of the principlse of CT principle and explains why the CT scanning procedure gained its popularity over a traditional X-ray imaging. Some known advantages and disadvantages of CT with respect to the medical usage are additionally listed. A brief overview of the characteristics of DECT data and the importance of noise reduction in the imaging pipeline of modern CT scanners is presented. Moreover, Chapter 2 provides an overview of some traditional noise reduction techniques in image processing. Chapter 3 deals with DECT related noise removal techniques and our implementations within the AngioVis framework. All of the algorithms are evaluated on CT data sets and a discussion of the final results is given in Chapter 4. Our work is concluded in Chapter 5 together with future aspects.

CHAPTER 2

Related Work

2.1 Computed Tomography

Computed tomography (CT) is widely used in medicine as imaging technique for medical diagnostic. Most medical surveys classify CT among the top five medical developments in last 50 years. The continued increase of its importance for medicine was a driving factor for many companies to jump on the diagnostic imaging industry which is still expected to grow. According to a recent pharmacy report, the global CT systems market will be worth $8.6 milliard by 2022 [4].

Standard radiographic techniques or X-ray imaging has some important limitations which can be surpassed by using CT. One important limitation of conventional X-ray imaging is that we are picturing a three-dimensional object but we project it (by superimposition) to a single two-dimensional plane, called a ‘radiograph’ or ‘photograph’, thus losing the volumetric representation of an object; the film (photographic plate) that is used as a medium for standard radiography is not able to capture fine contrast differentiation between different tissues. Thus the small differences in X-ray attenuation are not captured.

CT is able to provide a 3D representation of objects and 2D cross-sectional images or axial slices of the anatomy. High contrast and resolution is a very important characteristic of CT and thus important for medical diagnostic. CT is capable of differentiating between various types of tissue if they exhibit a difference in their physical density. As an example, in CT data sets one can easily distinguish between water and soft tissues, while in standard radiographic images tissues with similar attenuation are listed together (same gray value is assigned to both tissues).

Both, conventional X-ray imaging and CT, are based on the absorption of X-rays as they pass through different parts of human body. Depending on the part of body that is scanned, different constellations of tissues are present and thus different amounts of X-rays are absorbed. CT uses multiple 2D projections through 3D object and this allows the reconstruction of the objects in 3D space. CT also provides fine contrast differentiation between different types of tissue.

When it comes to single energy and dual energy CT, both generate data sets with the CT numbers at every voxel position. Those numbers represent spatial distribution of linear attenuation coefficients, and for the standardization they are given in the Hounsfield Units (HU).

By definition, for a given tissue with attenuation coefficient μ_g, HU number is calculated using equation [5]:

$$CT_{\text{value}} = \frac{\mu_g - \mu_{\text{water}}}{\mu_{\text{water}}} \cdot 1000\ HU \tag{2.1}$$

The mass attenuation coefficients of most tissues is energy dependent, i.e. HU numbers differ depending on the X-ray tube energy level that is used during scan procedure. However, HU numbers for water and air are constant, regardless of used tube voltage level and therefore are used as references. In the HU scale the water has value of 0 HU and the air is at -1000 HU.

2.2 Dual Energy Computed Tomography

Dual energy computed tomography (DECT) also called dual source computed tomography (DSCT) can be seen as extension of conventional single source computed tomography. Theoretically the concept of DECT is based on separation of the spectrum into two parts, a low energy part and a high energy part and the projection from two X-ray sources respectively [6]. Operational difference between standard CT (single energy) and dual energy CT is that standard CT uses only one X-ray source/detector pair which operating at one constant energy level, whereas dual energy CT uses two different energy levels.

There are two approaches in designing DECT systems. The first one uses a dual-source scanner and the second, one uses a single-source scanner with fast kilovoltage switching. Regardless of the scanner type the underlying principles are similar. They differ only in the way of how the data acquisition is done. Both dual energy approaches will generate two data sets, one recorded at a low energy X-ray spectrum and a second recorded at a higher energy X-ray spectrum. The energy levels for the low and high X-ray tube sources are often set at 80kV and 140kV respectively, but other configurations are possible, depending on the current study.

A virtual 120kV data set can be used as reference when comparing the DECT results with the features of a standard CT 120kV data set. This data set is generated as the weighted sum of the low and high energy data sets with 30% of 80kV and 70% of 140kV intensity values (an example is shown in Figure 2.2). This method is known as linear blending. Non-linear blending method can be used to further improve contrast-to-noise ratio (CNR) using a modified sigmoid function, as described by Holmes et al. [7].

Although the terms dual source and dual energy can be used interchangeably (both produce two different energy level data sets), it is important to note that not all dual energy CT systems use two X-ray tubes. Dual source CT in contrast to a single source CT consists of two rotating x-ray tubes and two digital detectors. Simple schematic diagram of a dual source CT system with illustrative example from the dataset used in this work is given in Figure 2.1.

As depicted in Figure 2.1, the signal from one x-ray tube can be detected only from one detector, placed on the opposite side. The patient is exposed to two energy levels; in this example (Figure 2.1), the low energy level is set at 100kV and the high energy level is set at 140 kV. With this technology two different energy level images are produced within a single scan. The acquired intensity values of the two data sets are different due to the different attenuation of materials exposed to the high and low energy levels. For example, in the low energy image bone

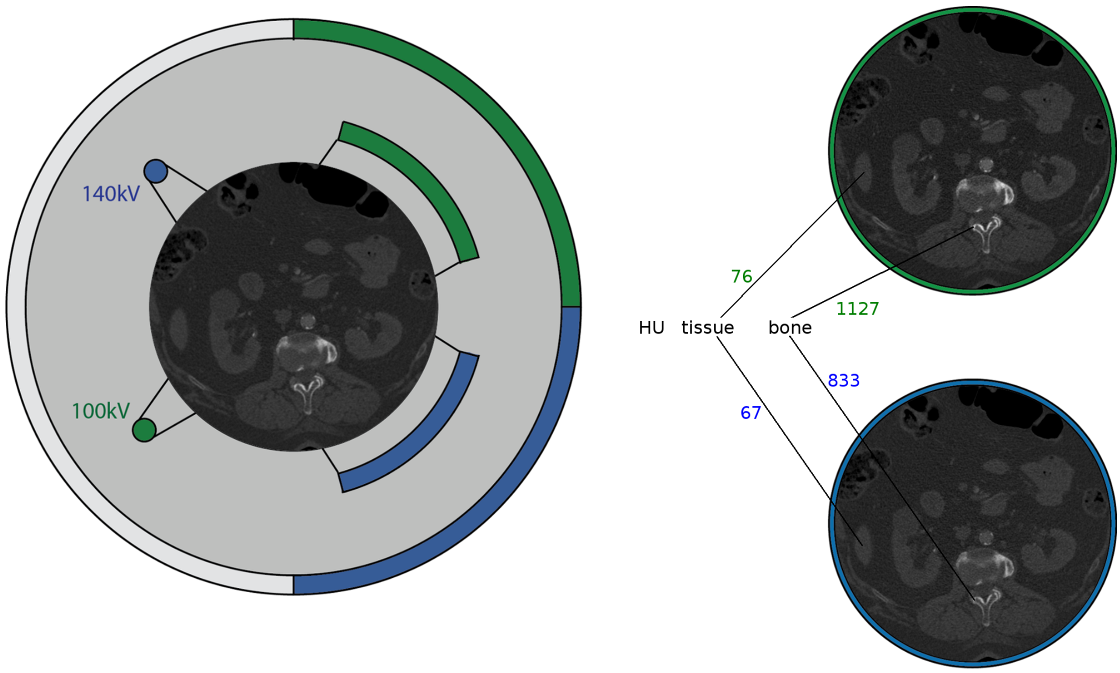

Figure 2.1: Schematic diagram of a DECT. Two separate scanners are used for the low 100kV and high 140kV energy level. The blue and green circles represent images acquired from different energy levels. The image in the left circle shows the blended one.

has the value of 1127 HU while in the high energy image the intensity value at the same spatial location is 883 HU. The different energy spectra provided by the two X-ray tubes, expose the patient simultaneously to the two different energy spectrums. An example of intensity values acquired using two tube voltages is given in Table 2.1.

By performing a comparison of the intensity values of both energy levels we observe how the HU values decrease as the energy of the X-ray increases. Higher energy X-rays penetrate easier through a highly dense materials than low energy X-rays, but as consequence the HU values are lower in the high energy image than the HU values at corresponding positions in the low energy image. Note that due to noise many intensity values are not following this trend of energy dependent material attenuation. One of the goals toward better noise reduction is to explore spectral information in order to find and correct the intensity values that do not follow the principle of energy dependent attenuation.

Table 2.1 depicts signal values detected by a DECT scanner, that represent the intensity of the X-ray spectrum after passing through the patient's body. The left side shows HU values for the small part of the low energy image (100kV) and the right shows HU values from the corresponding part in the high energy image (140kV). In general the HU values in the low energy data set should be higher than the intensity values in the high energy data set. Discrepancies in HU values at same pixel/voxel positions be seen.

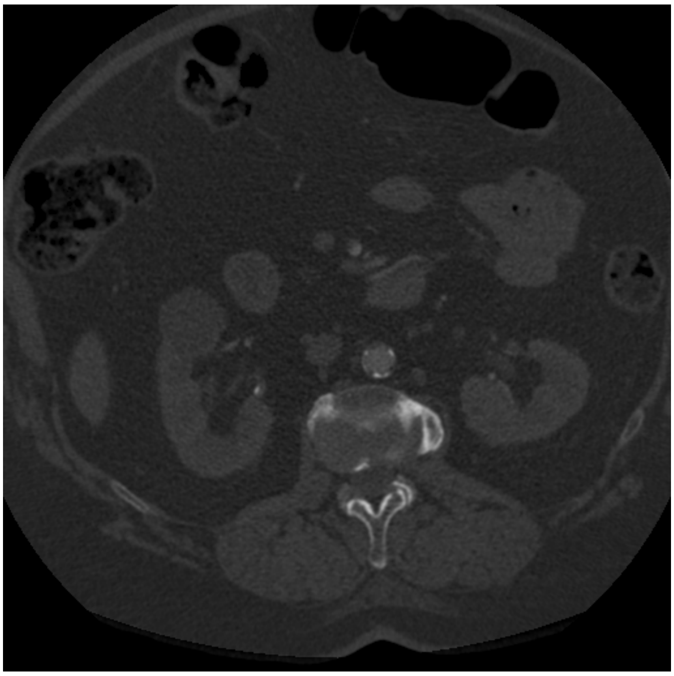

Figure 2.2: Virtual 120kV image

699	909	1012	971	777	547	398	396	531	700
472	795	1015	1044	933	773	623	576	674	826
297	658	942	1048	1018	912	780	757	864	998
167	477	796	971	988	928	887	936	1024	1078
67	338	658	840	849	850	943	1052	1094	1082
28	267	567	726	732	787	950	1068	1085	1078
39	225	490	664	712	771	906	1015	1065	1092
37	176	419	639	726	758	872	1037	1146	1141
26	157	408	657	759	761	884	1115	1225	1128
-5	111	360	636	777	797	913	1113	1164	993

(a)

593	745	783	745	650	465	274	249	359	485
362	579	779	882	841	663	465	437	545	676
152	398	688	869	870	741	618	640	738	819
66	290	558	727	759	713	698	762	837	868
52	252	482	615	655	674	719	797	856	872
28	221	442	565	591	609	677	776	838	855
1	176	409	559	568	537	622	774	866	862
-4	135	365	547	558	508	611	807	911	869
0	111	322	505	542	516	611	795	884	799
1	111	309	493	568	555	604	745	809	682

(b)

Table 2.1: (a) shows the intensity values of the low energy data set, whereas (b) the ones of the high energy data set. Both represent the same spatial location.

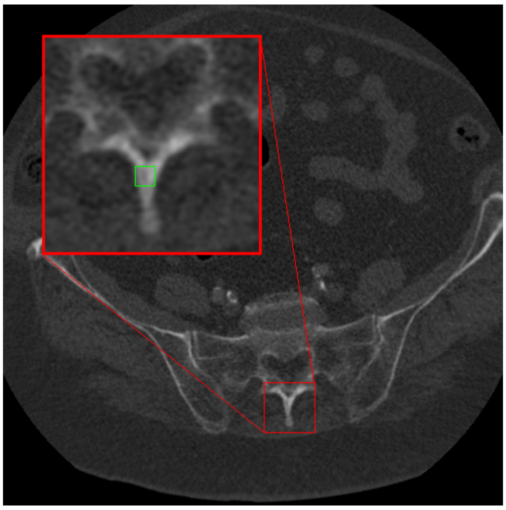

(a) Low energy image (100kV)

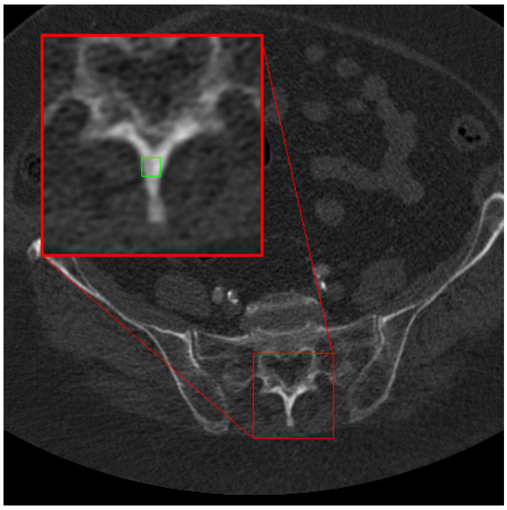

(b) High energy image (140kV)

Figure 2.3: An axial slice images of a DECT data set. Details are presented in the zoom-ins and the intensity values of the regions highlighted in green are shown in Table 2.1

Two images from the same DECT scan are shown in Figure 2.3. Both images have a resolution 512x512 pixels. The x-ray tube for the low energy image was set at 100kV and at 140kV for the high energy image. The data values from the green squares are exported into Table 2.1.

2.3 Computed Tomography in Medicine

One disadvantage of CT compared to the conventional X-ray imaging is that it involves a higher radiation dosage. However due to its medical diagnostic importance in diagnosis of cancer, cardiovascular and neurological diseases, the number of CT scans is constantly increasing. According to CT Market Outlook Report for US in 2007 there were 72 million scans, and in 2012 the estimated amount was 85 million scans. About 0.4% of cancer diseases in US in the year 2007 are due to the exposure to radiation with a dosage similar to today's CT scanners [8]. In a few decades up to 2% of all cancer diseases may be caused by the radiation exposure during CT scans. This estimate can be considerably lowered by avoiding medically not warranted CT scans [9]. There are also diverging beliefs that the CT irradiation dose is not sufficient and will not lead to a cancer formation. Several parameters influence the radiation dosage such as the patient's physique, the volume scanned, the desired resolution etc. Modern CT systems allow for auto adjustment of the exposure levels, which is a desirable feature, because it can help reducing the radiation dosage.

Another matter of importance related to the CT is the usage of radiocontrast agents, used to improve the visibility of internal bodily organs in CT data sets. Radiocontrast agents can cause serious anaphylactic reactions and other side effects, as described in the work of Lasser et al. [10]. Almost one half of all CT scans in US include some sort of radiocontrast agent, and according to recent statistics 2-30 people per 1,000,000 die from reactions caused by radiocontrast agent [11]. Radiologists should be aware of possible risk factors when using radiocontrast agents. Each patient is treated separately and an assessment of appropriate contrast agent prior to administration should be considered [12].

Compared to single energy CT the patient radiation dosage is in general equal or higher in DECT, however with technical improvements and additional mechanism it is possible to reduce the radiation dosage down to the level of single energy CT, or even lower [13].

DECT provides important new functional and specific information offering potential new applications in a number of medical areas. Cardiac imaging benefits from improved temporal resolution provided by DECT, making a functional evaluation of the heart valves and myocardium possible, as presented in the work of Seidensticker and Hofmann [6]. DECT is very often used for more accurate material differentiation and density measurement. Unique energy-dependent profiles are basis for material differentiation [14]. In other words, DECT methods exploit the difference in the mass attenuation coefficients of different materials as a function of energy. As an example, the differentiation of collagen makes it possible to depict tendons and ligaments, as mentioned by Flohr et al. [15]. Further examples show how the DECT can automatically separate bones and iodine-filled vessels or determinate stone composition [15]. Stones composed of different calcium salts can be more effectively detected, as described by Matlaga et al. [16].

2.4 Noise Reduction

Noise is a common problem in a variety of image processing scenarios. Noise reduction helps providing a more accurate digital representation of objects scanned by CT. In medicine, reducing unwanted noise of CT images is an important part of the examination of the patient's data set.

Typical noise reduction filters like median, average and Gaussian do not take pixel intensity distances (differences in pixel intensity values) into account during processing, which can produce unwanted effects like loss of image sharpness, and secondly they do not preserve edges. The bilateral filter offers both of these features.

Median Filter

The median filter is a non-linear filter, meaning that the pixel intensities are not linearly combined. All pixels of the filter kernel including the central pixel are sorted ascending by their intensity values and the middle element (i.e. the median) is chosen. The middle element is then saved in the output image at the position of the central pixel. The number of pixels that should be sorted depends on the size of the filter kernel. The run-time complexity of the median filter relative to the kernel depends on the chosen sorting algorithm.

An example of median filtering with a kernel size of 3×3 is shown in Table 2.2.
Central pixel value: 125
Kernel: -4, 135, 365, 0, 125, 322, 402, 111, 309
Sorted: -4, 0, 111, 125, **135**, 309, 322, 365, 402
Median: 135.
Filtered pixel intensity is 135, changed from 125.

-4	135	365
0	125	322
402	111	309

Table 2.2: An example of a 3×3 median filter kernel with the corresponding pixel intensity values.

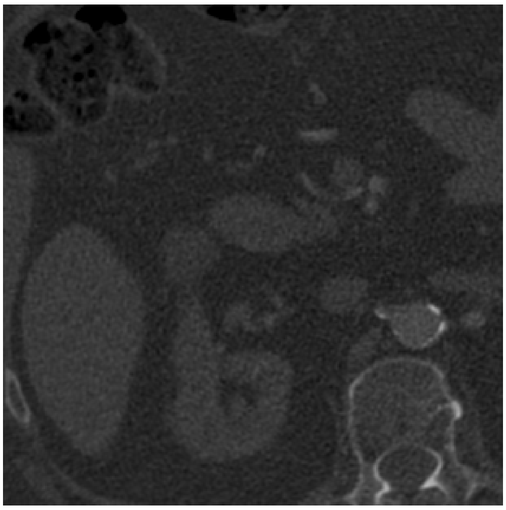

(a) Original image

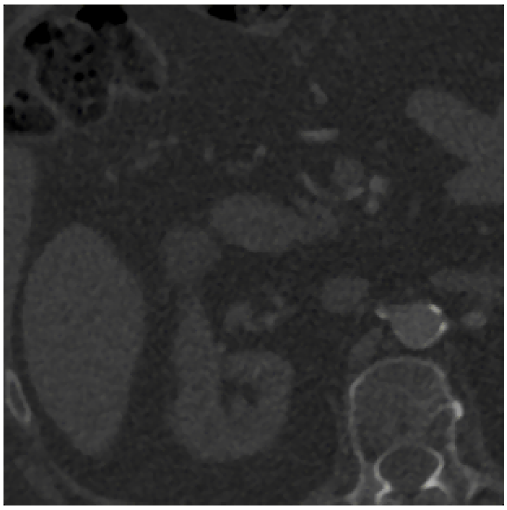

(b) Median filtered image

Figure 2.4: Example of a median filter. (a) shows the original image and (b) presents the median filtered version using a 5x5 kernel

Cons: Structured regions are smoothed and edges are blurred.
Pros: Edges between homogeneous regions are preserved. It preserves details better than average filter. Particularly good for salt and pepper alike noise.

Gaussian Filter

The Gaussian low-pass filter is widely used linear smoothing filter that can be applied straightforward on a CT images. The result is calculated through linear combination of all pixel intensity values inside the filter kernel. The Gaussian low-pass filter works in the spatial domain (it considers only the spatial distance from central pixel) and reduces noise effectively, but leads to smoothing that removes thin edges or smears them. An example of too much smoothing in the CT imaging would be when thin blood vessels disappear due to applying a Gaussian filter with a big standard deviation (σ). Filter kernel is calculated as follows:

$$G_{ND}(\overline{x};\sigma) = -\frac{1}{(\sqrt{2\pi}\sigma)^N} \cdot e^{-\frac{|\overline{x}|^2}{2\sigma^2}} \tag{2.2}$$

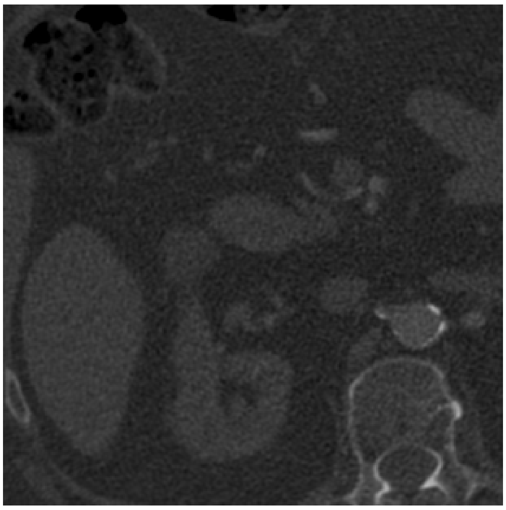

(a) Original image

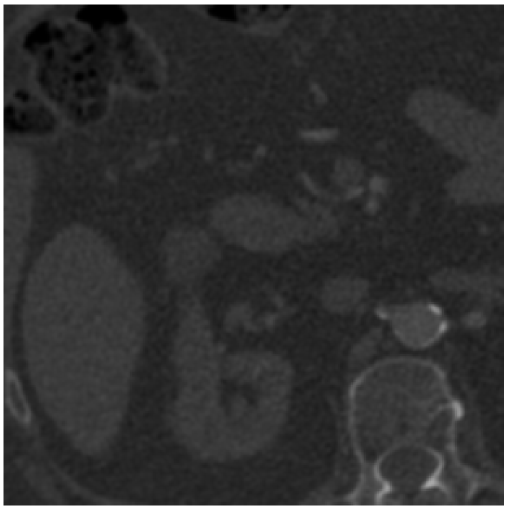

(b) Gaussian filtered image

Figure 2.5: Example of a Gaussian filter. (a) shows the original image and (b) presents the Gaussian filtered version using a 5×5 kernel with $\sigma = 1$

The sigma parameter determines how much the neighboring values from the central pixel influence the output pixel. A small sigma value means that distant pixels have less influence to the central pixel, while a big sigma value makes the influence of distant pixels significantly bigger to the result and leads to a greatly smoothed region.

0.002969	0.01331	0.02194	0.01330	0.002969
0.01331	0.05963	0.09832	0.05963	0.01331
0.02194	0.09832	0.1621	0.09832	0.02194
0.01331	0.05963	0.09832	0.05963	0.01331
0.002969	0.01331	0.02194	0.01331	0.002969

Table 2.3: 2D Gaussian filter kernel with $\sigma = 1.0$, after normalization

Cons: Edges are not preserved.
Pros: Does not have anisotropy property, i.e., filters edges of the same intensity values equally when they have a different orientation [17]. Higher frequencies are at all times more smoothed than lower frequencies, regardless of their direction.

Average Filter

The average or mean filter also belongs to the category of linear filters. The creation of the kernel is simple because all of its elements are set to a constant value. Using a symmetrical kernel of the size 5×5, the constant value would be 1/25, as shown in Table 2.4.

After convolving the average filter kernel with the input image, an example is presented in Figure 2.6.

$\frac{1}{25}$	$\frac{1}{25}$	$\frac{1}{25}$	$\frac{1}{25}$	$\frac{1}{25}$
$\frac{1}{25}$	$\frac{1}{25}$	$\frac{1}{25}$	$\frac{1}{25}$	$\frac{1}{25}$
$\frac{1}{25}$	$\frac{1}{25}$	$\frac{1}{25}$	$\frac{1}{25}$	$\frac{1}{25}$
$\frac{1}{25}$	$\frac{1}{25}$	$\frac{1}{25}$	$\frac{1}{25}$	$\frac{1}{25}$
$\frac{1}{25}$	$\frac{1}{25}$	$\frac{1}{25}$	$\frac{1}{25}$	$\frac{1}{25}$

Table 2.4: Average filter mask

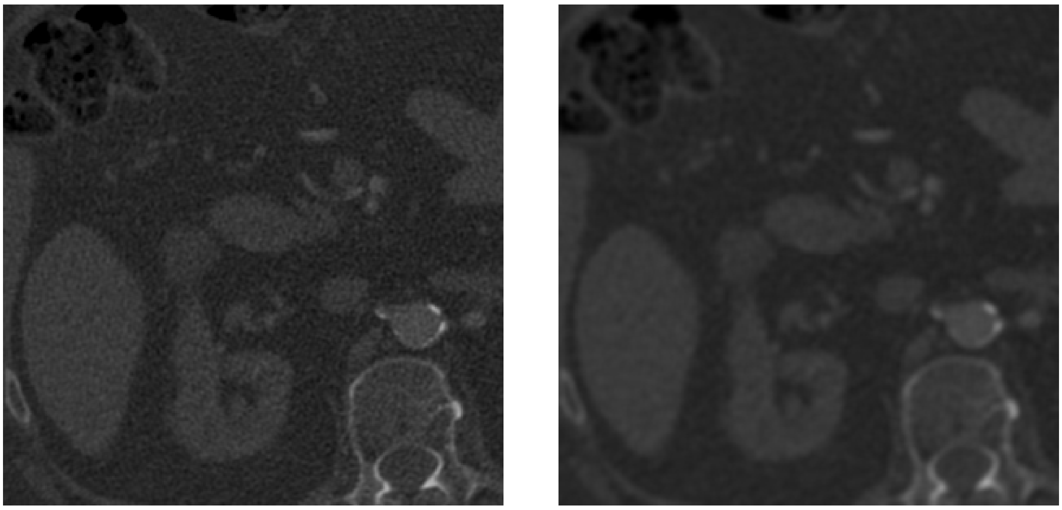

(a) Original image (b) Average filtered image

Figure 2.6: Example of a average filter. (a) shows the original image and (b) presents the average filtered version using a 5×5 kernel

Cons: If the pixel intensity values of the noise varies too much from the values of neighboring pixels, the average filter will not reduce much of the noise, and the image becomes blurry, because the mean value of the kernel is greatly changed. Another disadvantage of the average filter is the smoothing of sharp edges, and the resulting image loses high frequency details, meaning the edges are softened. The average filter does not filter edges of the same intensity values equally when they have a different orientation. This filtering property is known as anisotropy, as stated by Burger and Burge [17].
Pros: The average filter is often used for noise reduction because it is easy to implement.

Bilateral Filter

The bilateral filter belongs to the category of non-linear and edge preserving filters. In additional to the spatial information used by the Gaussian filter, it also takes the pixel intensity differences into account. This second intensity weighting is an important part of the algorithm because each value in the filter kernel is multiplied not only by the spatial weight as in the Gaussian filter but also with the intensity weight. As a consequence, the pixels with high intensity difference do

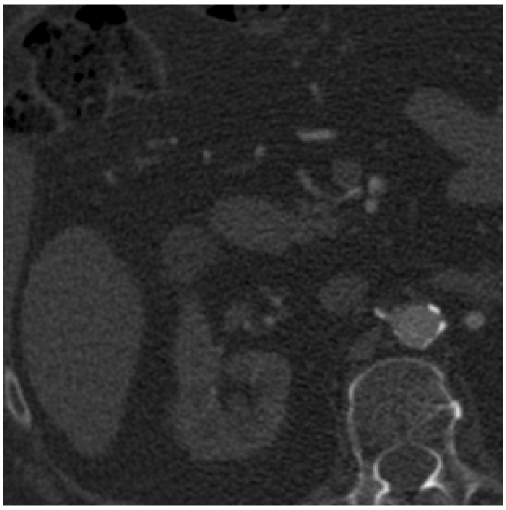

(a) Original image

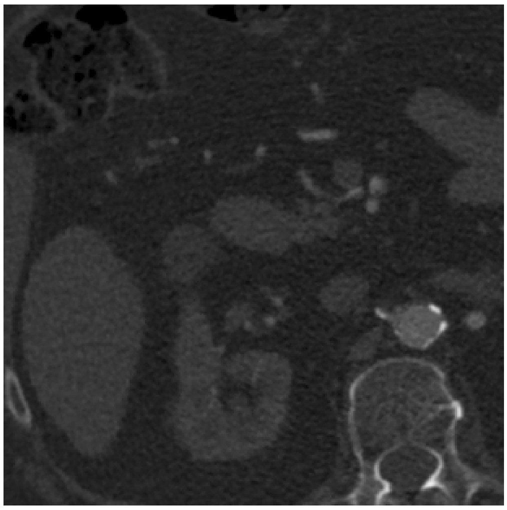

(b) Bilateral filtered image

Figure 2.7: Example of a bilateral filter. (a) shows the original image and (b) presents the bilateral filtered version using a 5×5 kernel, with σ_s = 1.0 and σ_r = 2.0

not influence the result that much as the pixels with small intensity difference. This leads to the preservation of edges and thin structures. Because of the intensity weighting part of the bilateral filter, edges do not influence surrounding homogeneous regions during smoothing process, and the image does not lose sharpness. Usually, the bilateral filter is applied on a single image but it can be easily expanded to two images that depict the same scene but with different extrinsic properties such as surrounding light intensity, slightly different angle (stereo images) or for the DECT images. In this work, we will implement a variation of the bilateral filter that is also known as joint or cross bilateral filter in image processing. The bilateral filter is described in more detail in Section 3.5, where it is applied on DECT data.

Cons: Computationally more demanding compared to average, median or Gaussian filter.
Pros: Popular choice amongst various smoothing filters because it preserves edges, hence, leaves the structured regions undistorted. Spatial parameter σ_s and intensity range parameter σ_r enable fine adjustment of smoothing.

2.5 Noise Reduction in DECT

The easiest way to effectively reduce noise in the CT imaging is to use higher energy levels for the CT scanning of the patient. However, this is not common practice, because the patient is exposed to an increased radiation dosage. In general, common noise reduction techniques, such as bilateral, Gaussian or median filtering can be applied on regular CT data sets, but due to the specific nature of the DECT imaging (two data sets of the same region but with different intensity values), several specific algorithms have been developed. Popular methods for noise reduction in the DECT imaging are the KCNR, noise clipping (NOC) and edge-predictive adaptive smoothing (EPAS) filter, as described in the work of Warp and Dobbins [18].

As stated by Kalender et al., the KCNR algorithm exploits the fact that noise in two energy levels is anti-correlated [2]. In the following chapter the KCNR algorithm is explained in more details.

Spectral information of DECT data is the difference between low and high energy data sets. This information is used in this work for the spectral-error correction [1]. The KCNR provides better results after applying it on the images with corrected spectral information. The bilateral filter can be also effectively used for noise reduction using DECT data. The first part of the bilateral filter, namely the spatial part, uses the distance information from the low energy image, while the second part of the algorithm (range part), uses the intensity information from the high energy image.

CHAPTER 3

Methodology

DECT offers new possibilities for innovative noise reduction techniques with the help of the additional spectral information. This information can be found in the difference between pixel intensities of two energy level data sets, as stated by Park et al. [1].

An example of input data sets used in this work is shown in Figure 3.1. It shows two axial slice images where the left image is from the data set generated using lower X-ray energy and the right image is from the data set generated using higher X-ray energy.

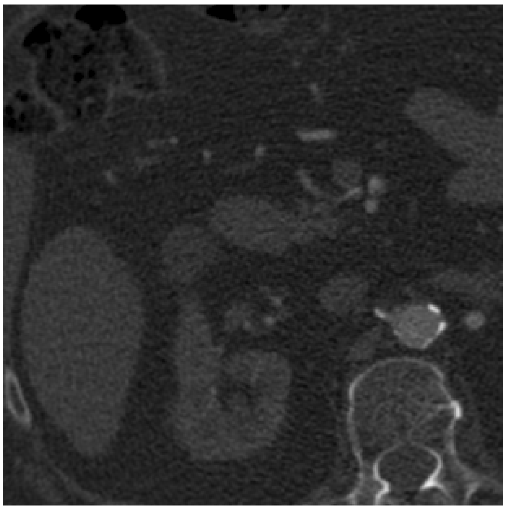

(a) Low energy

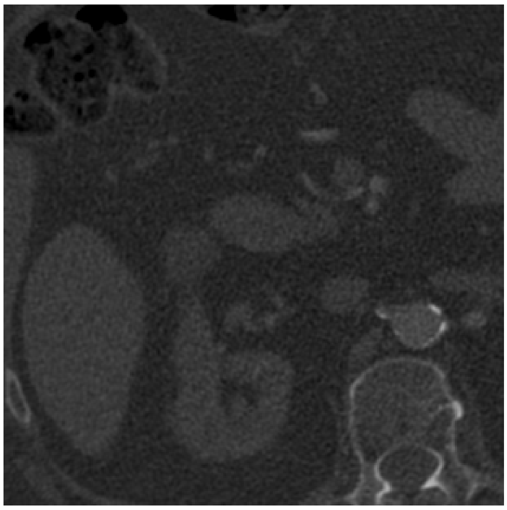

(b) High energy

Figure 3.1: Axial slice images of a DECT data set. Example of DECT data. (a) shows a slice image of the low energy data set (acquired at 100kV) and (b) presents the same slice image of the high energy data set (acquired at 140kV). The low energy image has higher contrast but the high energy image has less noise.

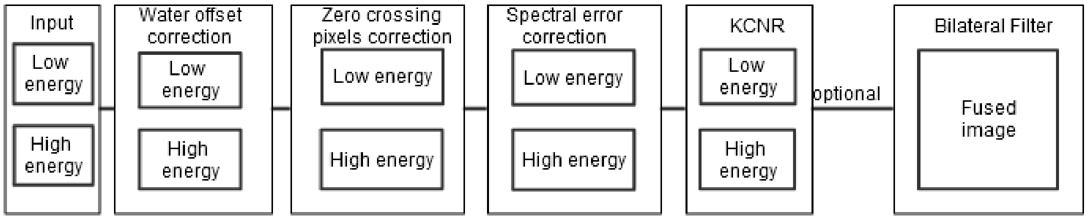

Figure 3.2: Diagram of the noise correction pipeline for DECT images.

In this Chapter we describe a pipeline (see Figure 3.2) for noise reduction in medical DECT data. As input, two energy level data sets are required. Data sets used in this work are consisting of axial cuts (slices). The implemented pipeline works with a volumetric data, and it is implemented slice-wise. All implemented techniques in our pipeline operate on both energy level data sets and the final output is again two data sets, with the noise reduced and edges preserved.

CT data sets we are using in this work are computed using standard back projection method. This means that energy- and material-selective reconstruction is not performed.

The water-offset correction algorithm corrects the HU values at the pixel positions that are supposed to be water with an intensity value of 0 HU, but their actual intensity values are higher than the user defined tolerance parameter (allowable deviation from 0 HU), as explained in the Section 3.1.

Zero-crossing pixels appear in the form of salt and pepper noise. They can effectively be removed using a standard median filter, as described in Section 2.4. We classify pixel pairs as zero-crossing if the following equation is true: $P_L \cdot P_H < 0$, where P_L and P_H are the pixel intensities of the low and high energy images respectively.

The spectral-error correction algorithm, together with the zero-crossing algorithm, aims to correct the pixel intensity values that do not follow the expected trend of attenuation, as explained in Section 3.3. This is an important part of the overall pipeline because noise is isolated and can be efficiently removed with the subsequent KCNR algorithm. The spectral-error is detected in the pixel pairs that satisfy the following equation: $P_0(P_L - P_H) < 0$, where P_0 represents the virtual 120kV image. However, a contribution of the fatty component in the tissue affects the strength of the change of the HU value, depending on the X-ray energy. This means that false positive spectral-error pairs are also possible. Thus, it is advisable to use the a parameter to restrict the spectral-error correction only on the pixel pairs when their difference exceed the user-specified tolerance.

The bilateral filter is optional and it can be applied prior or after the mentioned pipeline is executed. It takes two data sets as input and produces a single, combined data set as output.

3.1 Water-offset Correction

Even when the CT scanner is calibrated by using a phantom before the actual imaging process, the water references appear to be biased, sometimes over 10 HU, especially in the low energy data set [19]. Therefore, a water correction is usually done in the image-processing algorithm directly on the CT scanner. However, by studying the test data we observed that some intensity values still need a water-offset correction, as shown in Figure 3.3.

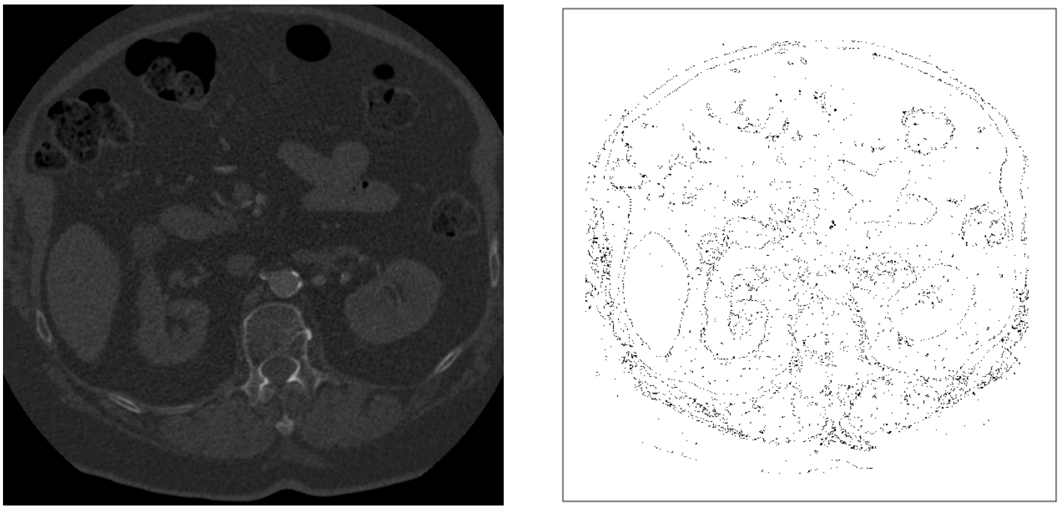

(a) (b)

Figure 3.3: Water-offset correction. (a) shows the original image, (b) presents only the water-offset corrected pixels.

Water in the CT data is like air unaffected by the change of the CT energy level, as stated by Park et al. [1]. In other words, the CT values of the water-reference are not dependent on the X-ray energy level and stay always closely around 0 HU. However, mostly due to the quantum noise, beam hardening and scattered radiation, the water references are biased and the values for water vary mostly in the range from -10 HU to 6 HU [5]. In order to correct the water-reference offset we need a reference to compare with, and in practice the virtual 120kV image is used as the reliable source; As explained in Section 2.2, the virtual 120kV image is a weighted blend, or linear combination of the low and high energy level images, using 30% of the 100kV and 70% of the 140kV images. The virtual 120kV image is supposed to have accurate intensity values of water, even when the low and high energy images are biased, as stated by Park [19]. Using the virtual 120kV image as the trustworthy reference, erroneous pixels are recognized (see Figure 3.3) in the low and high energy images and corrected if they surpass a user-specified tolerance intensity value. In our experiments we use intensity values of -10 HU for the negative and 6 HU for positive tolerance respectively. Note that the ratio of the corrected water-reference offset pixels in the low and high energy images to the total number of pixels in the images is relatively low, meaning that correction is barely visible and noticeable in our test data sets. The majority of the detected water-like pixels is located on the boundaries of different types of tissue.

3.2 Zero-crossing Pixels Correction

When zero-crossing pixel pairs are present in DECT images they are visually manifested in the form of salt and pepper noise or spike-like noise that can distort the final image, as stated by Park et al. [1]. Zero-crossing pixel pairs are determined by examining a pair of pixels, where one is taken from the low energy and another from high energy image, and verified whether they meet the criteria of the following equation,

$$P_L \cdot P_H < 0 \tag{3.1}$$

where P_L and P_H are pixel intensity values of the low and high energy images respectively. In other words, if the result of the multiplication of two intensity values is negative, instead of being positive, then such pixel pairs are called zero-crossing pixels. They are corrected before the spectral-error correction. The zero-crossing pixel pairs in the low and high energy images are replaced with the median of their respective 3×3 neighborhood.

3.3 Spectral-error Correction

Spectral-error correction is the most important part in the correction process of our pipeline (see Figure 3.2). The spectral-error correction algorithm is based on the fact that the attenuation of a highly dense material decreases more rapidly than the attenuation of materials with low density, with increasing CT tube voltage. Pixel pairs that deviate from the expected trend of Equation 3.2 are treated as spectral-error,

$$P_0(P_L - P_H) \geq 0 \tag{3.2}$$

where P_L and P_H are pixel intensities of the low and high energy images respectively, and P_0 is the intensity value of the virtual 120kV. All spectral-error pixel pairs detected in previous step are corrected with new intensity values P'_L and P'_H, for low and high energy data set respectively, calculated using following equations:

$$P'_L = 0.3 \cdot P_L + 0.7 \cdot P_H \tag{3.3}$$

$$P'_H = 0.7 \cdot P_L + 0.3 \cdot P_H \tag{3.4}$$

It is important to note that the criteria for the spectral-error can not be generalized, for example, some types of tissue have increased CT values, depending on the distribution of fatty components, and therefore, the spectral-error pixels should be replaced only if the difference of the intensity values of the pixel pair exceeds a certain tolerance, as described by Park [19].

The intensity values from the green squares shown in Figure 3.4 are illustrated in the graphs in the middle Figure. The final result of the spectral-error correction algorithm is shown in Figure 3.5. Random noise is still present, which will be removed in the next step with the KCNR.

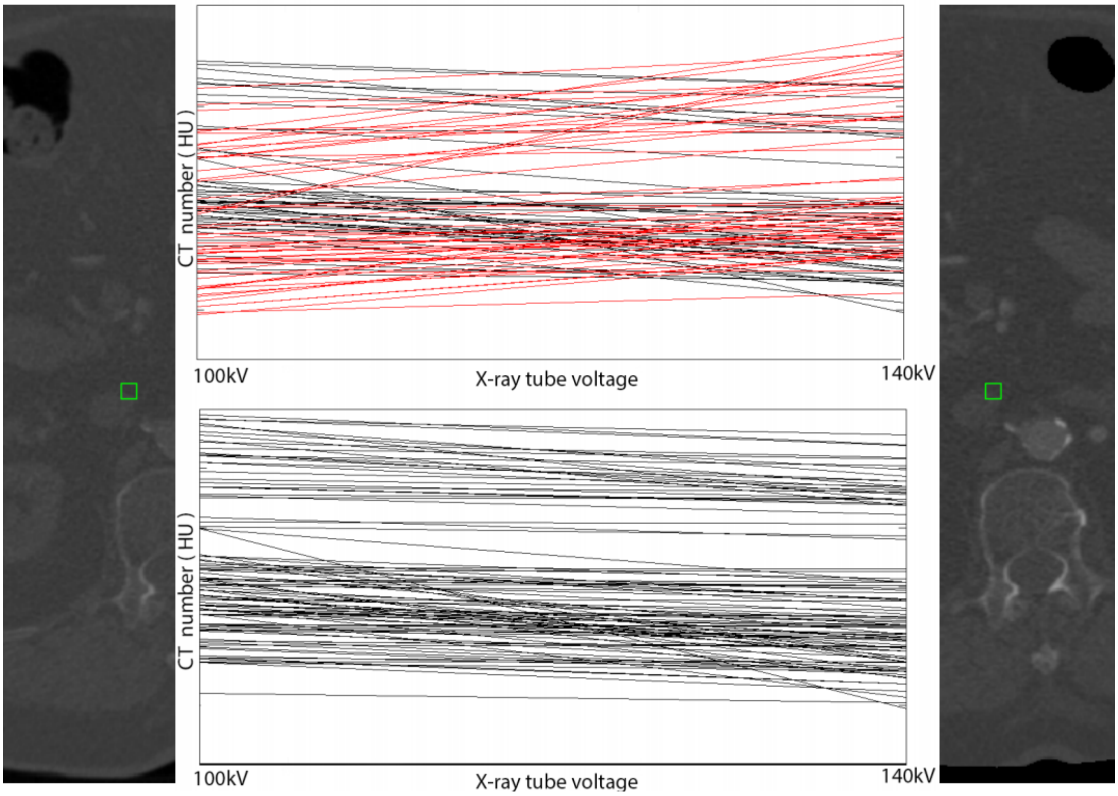

Figure 3.4: The intensity valued of the areas highlighted by the green squares in the left (low energy) and right (high energy) CT images are shown in the central graphs. The top graph shows the intensity values before the spectral-error correction, whereas the bottom graph after the correction. The vertical axis of the graphs shows the pixel intensity values measured in HU, for the 100kV (left) and 140kV (right) energy levels. Pixel pairs of the low energy (100kV) and high energy (140kV) images are connected with lines from left to right. The red lines represent a spectral-error, meaning that these pixel pairs do not follow the trend of the expected material attenuation $P_0(P_L - P_H) \geq 0$. According to this expectation, the intensity values of the low energy image should be always higher than the intensity values of the high energy image.

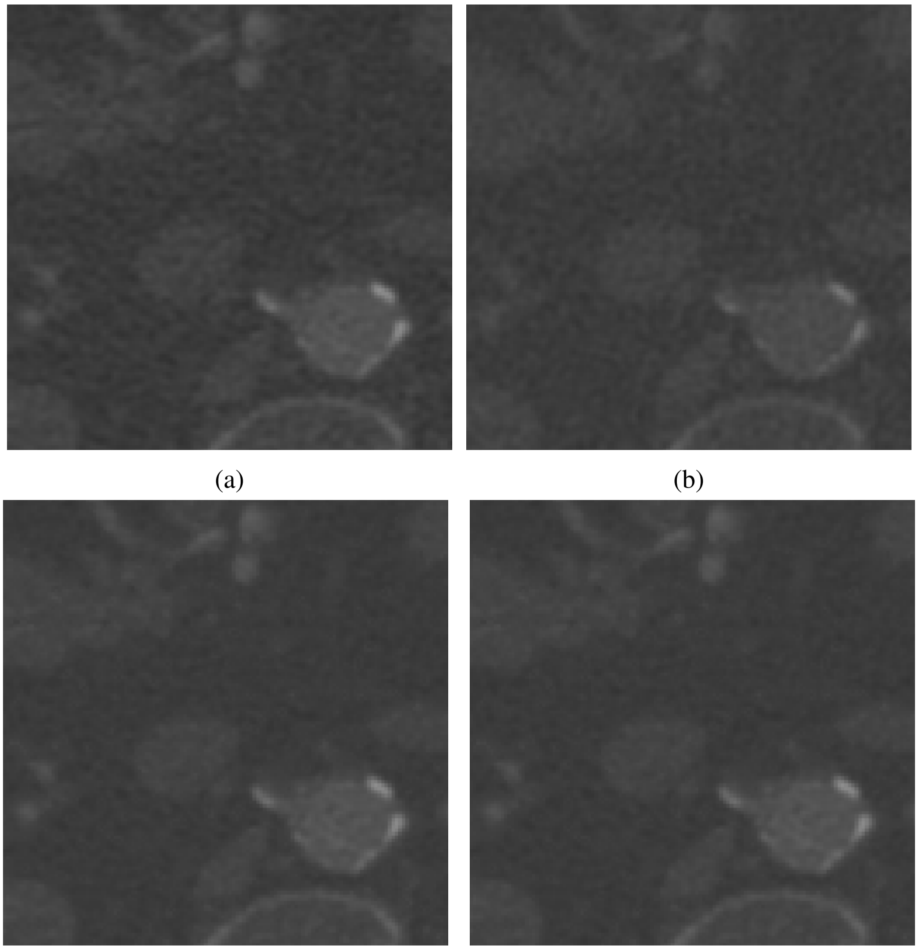

(a) (b) (c) (d)

Figure 3.5: Results of the spectral-error correction in both energy levels. (a) shows the original low energy image, (b) the original high energy image. (c) shows the low energy image after the spectral-error correction, (d) the high energy image after the spectral-error correction.

3.4 Kalenders Correlated Noise Reduction

The KCNR is a reliable and efficient algorithm for decreasing noise in DECT data sets. It exploits the differences in intensity values between the low and high energy data sets and successfully reduces negatively correlated random noise, as described by Kalender et al. [2].

The KCNR, which is used in the last stage of our pipeline in order to reduce correlated noise, delivers better results when applied after the spectral-error correction [1].

First we calculate means $\overline{P}_L$ and $\overline{P}_H$ of the intensity values in the $n \times n$ kernels centered on the input pixels P_L and P_H from the low and high energy images respectively. Throughout our work we use a kernel of size 5×5.

In the next step differences between original pixel intensity values P_L and P_H and their related means $\overline{P}_L$ and $\overline{P}_H$ are subtracted and saved as ΔP_L and ΔP_H according to the Equations 3.5 and 3.6. This is equivalent to a high-pass filtered versions of original pixel intensity values.

$$\Delta P_L = P_L - \overline{P}_L \tag{3.5}$$

$$\Delta P_H = P_H - \overline{P}_H \tag{3.6}$$

If ΔP_L and ΔP_H are of opposite signs, the filtered versions P'_L and P'_H are calculated using the subsequent Equations:

$$C = (W_H \cdot \Delta P_H - W_L \cdot \Delta P_L)/2 \tag{3.7}$$

$$P'_L = P_L + C/W_L \tag{3.8}$$

$$P'_H = P_H - C/W_H \tag{3.9}$$

where C is the correction term, and W_L and W_H are weights. If ΔP_L and ΔP_H are of the same sign the correction term will have none or a very little effect.

Results of our pipeline, including the KCNR, are shown in Figure 3.6.

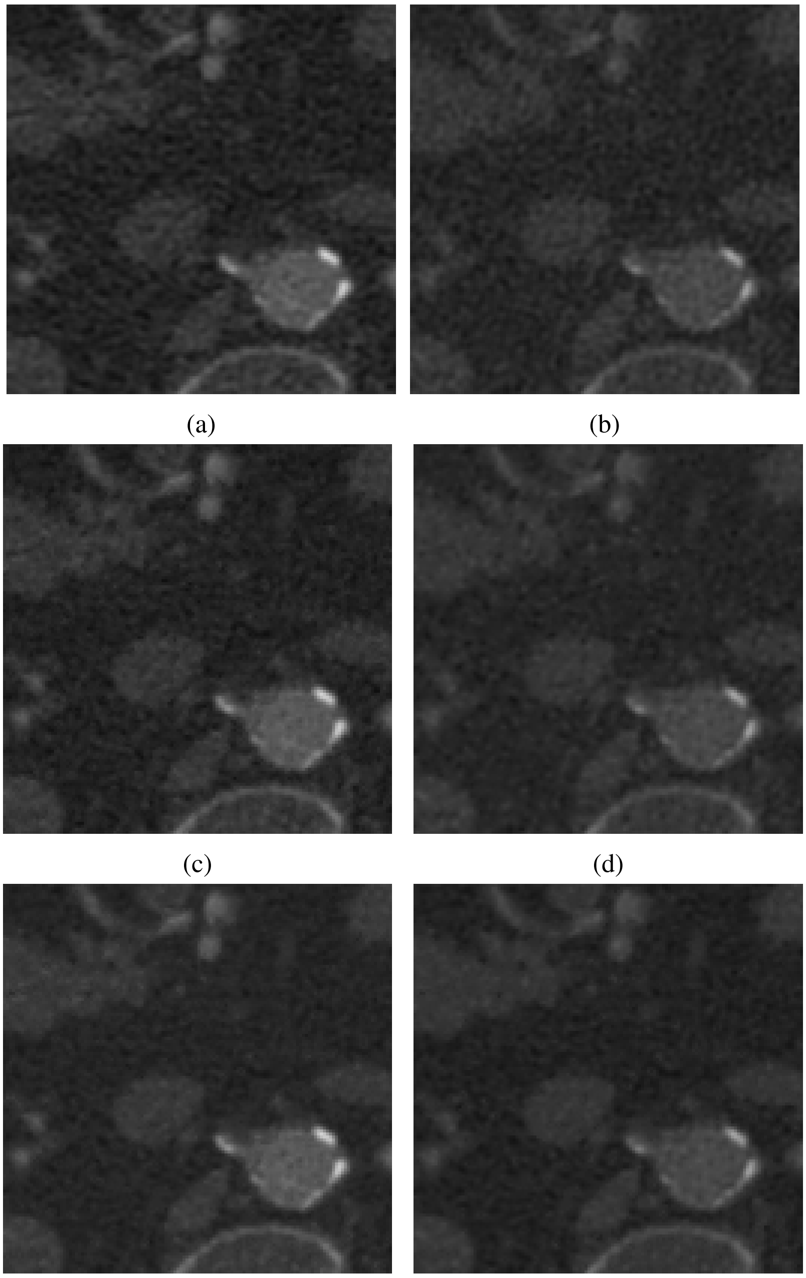

(a) (b) (c) (d) (e) (f)

Figure 3.6: Results of KCNR. (a) shows the original low energy image and, (b) the original high energy image. (c) presents the result of applying KCNR to the low energy image and (d) displays the results of KCNR for the high energy image. (e) and (f) show the results of KCNR when applied after the spectral-error correction, for the low and high energy images respectively.

3.5 Bilateral Filter

Noise in images can be effectively reduced by applying different smoothing filters. However, in many situations it is not desired to lose important details, like thin edges or sharp tissue boundaries. The question is how many details we want to preserve, because smoothing does not only remove noise but details too. This undesirable effect partly originates from the design of traditional smoothing filters. Most of the traditional smoothing filters operate in the spatial domain, i.e., they look only at differences of the distance to the central pixel.

Smoothing filters, including the bilateral filter, are mostly based on convolution. During the convolution, a smoothing filter accounts only for intensity values in the neighborhood of a central pixel. The neighborhood is defined by the filter kernel size, typically 3×3, 5×5 or 7×7.

Convolution means that we have a 2D filter kernel and a 2D image and the filter looks only for values in the neighborhood of the central pixel, where the neighborhood is defined by the filter kernel size (typically 3×3, 5×5 or 7×7). Usually the kernel size is odd, meaning there is always one central pixel. The output of the filter operation at certain location is given as weighted average of the neighborhood intensity values. As already mentioned, the proximity of the central pixel plays an important role.

The bilateral filter is also used for image smoothing and noise reduction but in addition it preserves edges. This is possible because in addition to the spatial domain it operates in the range domain, as described by Tomasi and Manduchi [20]. This means that not only the proximity of the central pixel in the spatial domain is important, but bilateral filter also accounts for pixels with similar intensity values. Neighbors of the central pixel that vary significantly in their intensity value are taken less into account during filtering. This method greatly succeeds in preserving edges of objects in the image, as shown in Figure 3.7. The bilateral filter is a noniterative nonlinear method proposed for single image filtering. However, it can easily be extended for two images, as proposed by Petschnigg et al. [21].

DECT uses two different X-ray energy levels and it generates two images which are registered to each other; image registration in DECT is very important because the intensity values at the same image pixel position in the low energy image and the high energy image must be correlated to each other. The bilateral filter can benefit from this correlation by using information from both images at the same time in order to reduce noise without smoothing the edges. An image taken at low X-ray energy has a large intensity range similar to what we get when we are taking a picture with a camera in a half-dark environment. In the low X-ray energy image we can easily distinguish various types of tissue, but it has a high amount of noise. The image taken at high X-ray energy is like an image taken with a flash, we get better details but the image has a narrower intensity range. The idea is now to combine these two images and thus gain a large scale of intensity values (contrast) from the low energy image, and details from the high energy image.

We implemented the bilateral filter for volumetric CT data, by considering neighborhood voxels along every axis. In the spectral part of the bilateral filter smoothing is done on the low energy images in order to remove noise, but in its range part the bilateral filter looks for pixel intensities in the high energy images, thus avoiding blurring of the edges and preserving details.

Two user-specified parameters, the spatial parameter σ_s and range parameter σ_r, influence the strength of the filtering. The spatial parameter has a direct influence on the estimation of the filter kernel size:

$$n_{\text{(kernel size)}} = 6 \cdot \sigma_s - 1 \tag{3.10}$$

by affecting the 3D Gaussian kernel in its geometric spread and size. The kernel is $3 \times 3 \times 3$ if the user inputs σ_s smaller than 0.666. The size of the kernel is rounded and adjusted to be odd. The range parameter dictates the edge preservation tolerance.

$$BF[I]_p = \frac{1}{W_p} \sum_{q \in S} G_{\sigma_s}(||p - q||)\, G_{\sigma_r}(|I_p - I_q|) I_q \tag{3.11}$$

$$W_p = \sum_{q \in S} G_{\sigma_s}(||p - q||)\, G_{\sigma_r}(|I_p - I_q|) \tag{3.12}$$

Convolution is done in 3D space and the kernel size defines how many neighboring slices of the volumetric data set have to be taken into account. The low energy image is smoothed with the spatial Gaussian weight (G_{σ_s}), at the same time, the edges are preserved using intensity details taken from the high energy image, with the so-called range Gaussian weight (G_{σ_r}) [22]. The range Gaussian weight is taken from the high energy image in order to decrease the influence of neighboring pixels q (in 3D), from central pixel p, when their intensity value I_q differs much from intensity value of central pixel I_p. A normalization step W_p ensures that the weighted sum of the pixels equals one (see Equation 3.12). The pseudocode of our DECT bilateral filter algorithm is shown in Algorithm 3.1.

The effectiveness of the noise reduction of the DECT bilateral filter is evaluated using the same DECT data set explained in the previous section. Filtering is done in 3D.

The amount of smoothing depends on the factor σ_s used in the calculation of the spatial part of the bilateral filter. As shown in Formula 3.10, the σ_s influences the kernel size. Results of the DECT bilateral filter using four different σ_s values, 1.0, 1.4, 1.7 and 4, are shown in Figure 3.7. From the images demonstrated in Figure 3.7 one can derive that the amount of blurring is directly proportional to σ_s.

The σ_r parameter is used only in the range domain of the bilateral filter but directly influences the strength and quality of the final smoothing result. We use six different σ_r values (2, 5, 10, 30, 100, 250). A small σ_r means that only the neighboring pixels with a small difference in intensity value (smaller than the σ_r) to the central pixel intensity are mixed together, and those whose intensity values are higher than σ_r are not. In other words, the range Gaussian part of the bilateral formula (see Equation 3.11) decreases the influence of the pixels in the neighborhood of the central pixel, whose intensity values I_q differ much from the intensity value I_p of the central pixel.

Figure 3.8 illustrates the smoothing effect of the larger σ_s values. When the kernel size is larger than 7×7, i.e. σ_s is higher than 1.7, the blurring is too much with the consequence that many edges are completely removed from the resulting image. Note that the appropriate parameter values, σ_s and σ_r, must be chosen depending on the anatomical region of interest.

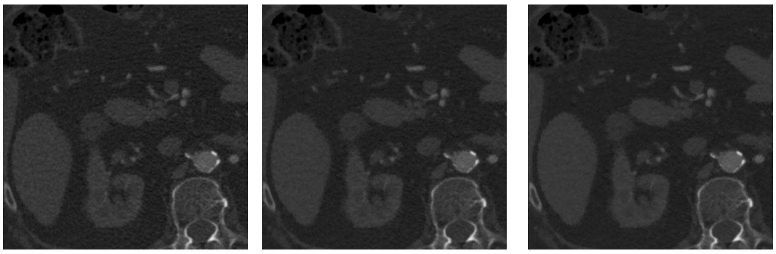

(a) σ_s=1, σ_r=2 (b) σ_s=1.4, σ_r=2 (c) σ_s=1.7, σ_r=2

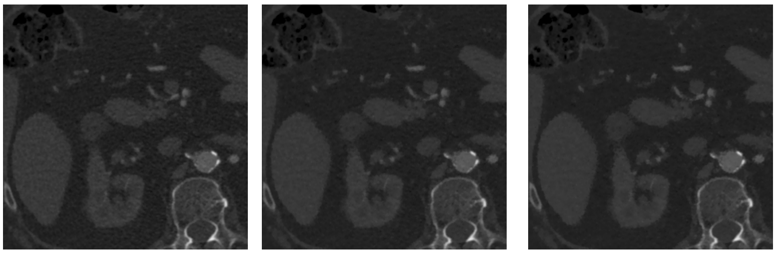

(d) σ_s=1, σ_r=5 (e) σ_s=1.4, σ_r=5 (f) σ_s=1.7, σ_r=5

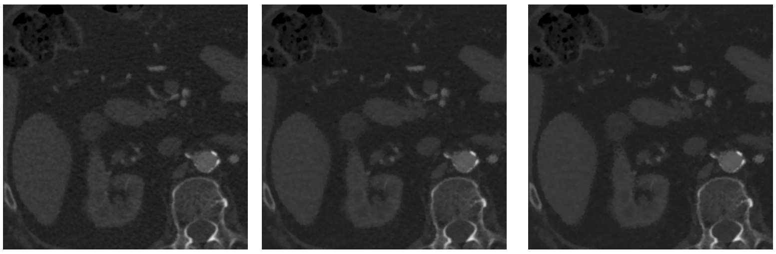

(g) σ_s=1, σ_r=10 (h) σ_s=1.4, σ_r=10 (i) σ_s=1.7, σ_r=10

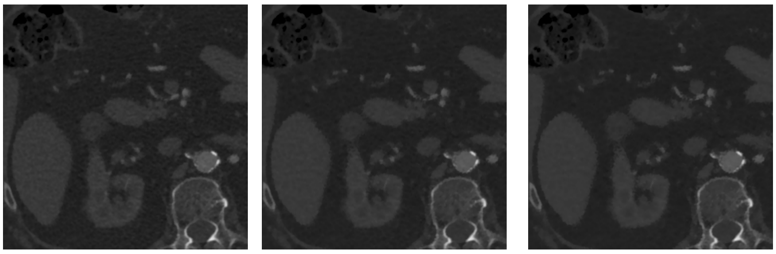

(j) σ_s=1, σ_r=30 (k) σ_s=1.4, σ_r=30 (l) σ_s=1.7, σ_r=30

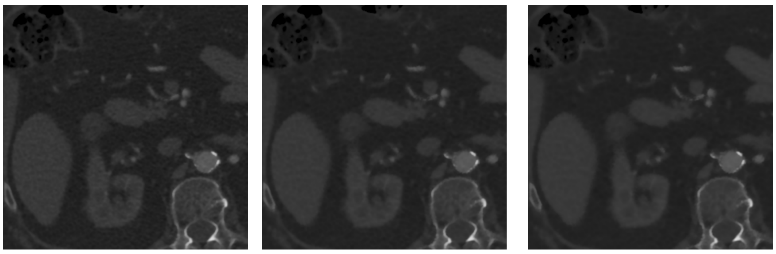

(m) σ_s=1, σ_r=100 (n) σ_s=1.4, σ_r=100 (o) σ_s=1.7, σ_r=100

Figure 3.7: The results of using different combinations of the σ_s and σ_r parameter values for the DECT bilateral filter.

Data: low energy volume L, high energy volume H, σ_s, σ_r
Result: volume O

```
/* input volumes and output have same dimensions */
3Dkernel = compute3DGaussianKernelMask(σ_s);
k = 3Dkernel.countOfElements() ;
foreach voxel position p in volume do
    normalizer = 0;
    sum = 0;
    I_high = voxel intensity at position H(p) ;
    Q_l = intensities of k neighbors for L(p) ;
    Q_h = intensities of k neighbors for H(p) ;
    for i = 1 to k do
        range_domain = e^(-|I_high - Q_h(i)|^2 / 2·σ_r^2)) ;
        spatial_domain = 3Dkernel(i) ;
        sum += range_domain · spatial_domain · Q_l(i) ;
        normalizer += 3Dkernel(i) · spatial_domain ;
    end
    outputVoxel = sum / normalizer ;
    save outputVoxel at O(p) ;
end
```

Algorithm 3.1: The pseudo-code of the DECT bilateral filter.

A σ_s smaller than 1.4 appears more appropriate for our tested slice of the abdominal DECT image, while keeping the σ_r parameter between 10 and 30.

Note that the computing time drastically increases for larger kernels. For the 3D Gaussian kernel of the size 23×23, computation time of the bilateral filter for one slice took nearly about one hour (on the Intel processor Core 2 Duo 2.1GHz). The result of this extreme smoothing is shown in Figure 3.8. Due to the very high σ_r parameter, the bilateral filter approximates the standard Gaussian smoothing because the range Gaussian widens and flattens.

We observed that noise reduction can be improved when applying a bilateral filter after the series of enhancement described in our pipeline (see Figure 3.2). As result a single fused image with clearly defined regions and drastically reduced noise is obtained.

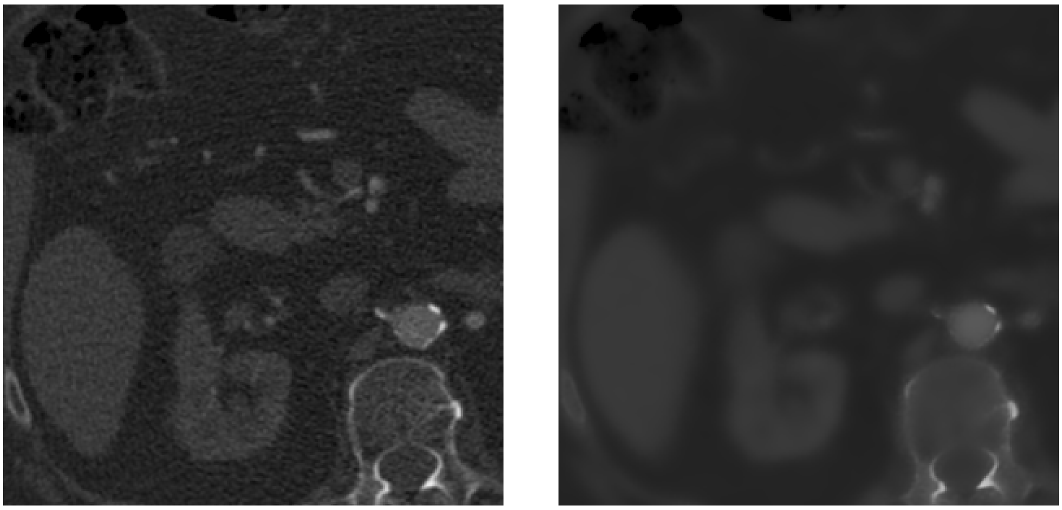

(a) Original image

(b) Filtered image

Figure 3.8: An example of the DECT bilateral filtering with very large parameter values ($\sigma_s = 4.0$, $\sigma_r = 250$).

CHAPTER 4

Results and Discussion

We applied our pipeline to medical DECT data sets without the given ground truth image and without doing two-material decomposition as it was done in the original proposition of the KCNR algorithm. KCNR algorithm can be applied on any DECT image independent of the spectral-error correction, however the results are better when the KCNR is applied on images with corrected spectral information [18]. We observed good results in noise reduction using KCNR.

Water-offset correction and zero-crossing pixels correction are also viable techniques for DECT imaging and we applied them in the course of spectral-error correction. Figure 4.1 shows the results of applying the spectral-error correction in combination with the KCNR algorithm. It is evident that noise is reduced and homogeneous regions are now more distinguishable.

The bilateral filter can be used as a stand-alone filter, or in combination with the presented noise reduction pipeline. For the bilateral filter it is necessary to adjust parameter values for the strength of the smoothing. In contrast to the implemented noise reduction pipeline where we have two data sets as output, the bilateral filter generates only a single, fused data set as output. Such a data set, as demonstrated on an axial slice image in Figure 4.2 (a) has improved contrast and less noise, compared to original data set shown in Figure 4.1 (a), but the boundaries between different types of tissue are distorted.

We observed that the bilateral filter produces the best results when it is applied on the data sets that have already been processed with KCNR, i.e., as the final step of the pipeline (see Figure 4.2 (b)). Boundaries between homogeneous regions are now clearly visible.

The jaggy boundaries between different regions, as shown in Figure 4.2 result from applying the DECT bilateral filter only, without the other steps of our pipeline. This can be explained with the range parameter, $\sigma_r = 10$, applied on the noisy original low and high energy images. Because the range parameter takes pixel intensity values around the central pixel into account, a large range parameter leads to a significant influence of the noise on the output intensity value. As we can see in Figure 4.5, applying the bilateral filter on the noise reduced images, even when the range parameter is large, $\sigma_r = 20$, the boundaries between different types of tissue are not jaggy.

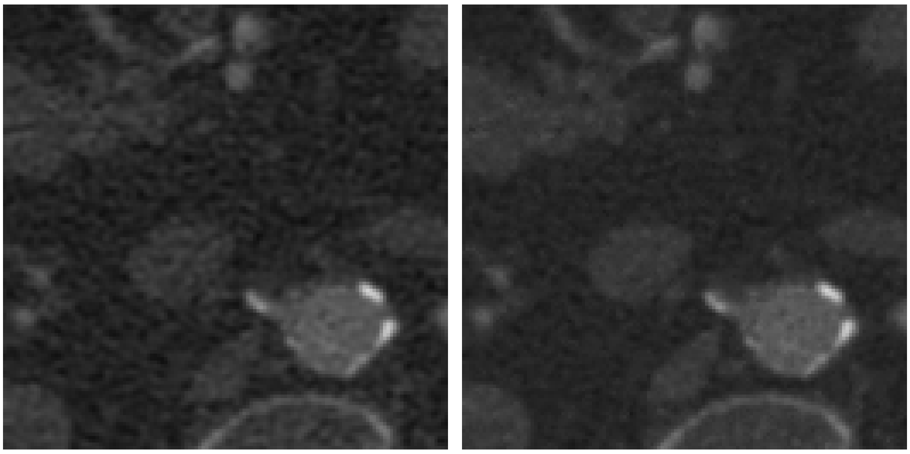

(a) (b)

Figure 4.1: Results of our noise reduction pipeline. (a) shows the original image and (b) after noise reduction and spectral error-correction, but without the final bilateral filter. One can clearly notice the reduced noise and the preserved edges of the structures in (b).

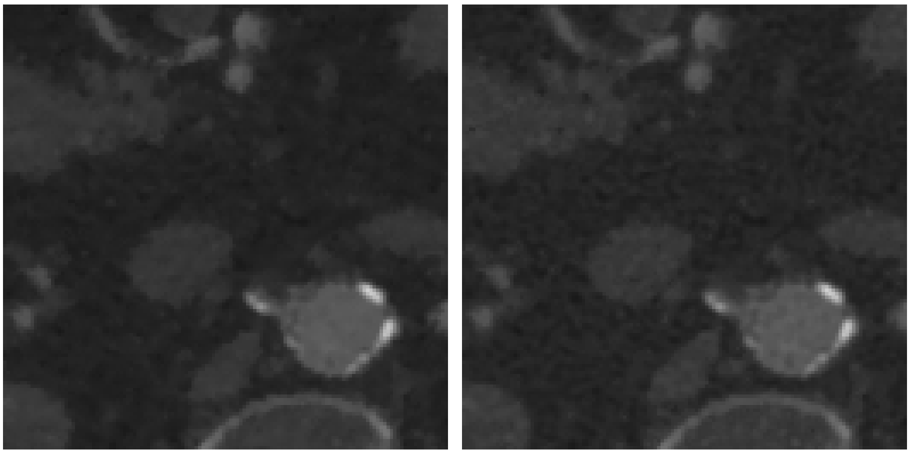

(a) (b)

Figure 4.2: Bilateral filtering with parameters: $\sigma_s = 1.4$, $\sigma_r = 10$. (a) shows the result of applying the bilateral filter on the original low and high energy images. The resulting image, so-called 'fused smoothed image' takes benefits from both energy images, i.e. the new image is a smoothed version of the low energy image with removed noise but preserved high contrast range, and the edges are preserved using the intensity information from the high energy image. The noise is mostly removed, but many regions have jaggy boundaries. (b) shows the result of applying the bilateral filter after correcting the spectral-errors and removing anti-correlated noise.

Figure 4.3 shows another slice of a DECT data set, in the pelvis region, processed by our pipeline. The psoas muscle in the input images Figure 4.3 (a) and (b) is not clearly defined due to noise. The same muscle is shown in the output image of our pipeline, but with less noise and higher contrast. Without the bilateral filtering, the output images of our pipeline, as shown in Figure 4.3 (c) and (d), have good contrast, but still a small amount of noise is present and spread across the images.

In Figure 4.4, we present a coronal slice images of a DECT data set. We compare the virtual 120kV image with final results of our pipeline. The virtual 120kV image is explained in Section 2.2. Comparing it to the original high energy image Figure 4.4 (a), we see that noise is mainly reduced and the contrast from the high energy image is preserved. Our pipeline, as demonstrated in Figure 4.4 (c), reduces the correlated noise, compared to the virtual 120kV image. In Figure 4.4 (d) we show that the DECT bilateral filter with parameters $\sigma_s = 1.5$ and $\sigma_r = 5.0$ improves the contrast compared to Figure 4.4(b), while still preserving the boundaries of different types of tissue.

We can clearly see benefits of using the bilateral filter in our pipeline, when comparing with the virtual 120kV image shown in Figure 4.5 (a) with the results of our pipeline, once without and once with the DECT bilateral filter. We observe that the result of our pipeline together with the DECT bilateral filter, shown in Figure 4.5 (c), has significantly less noise compared to Figure 4.5 (a) or (b), and the boundaries of different regions are clearly visible.

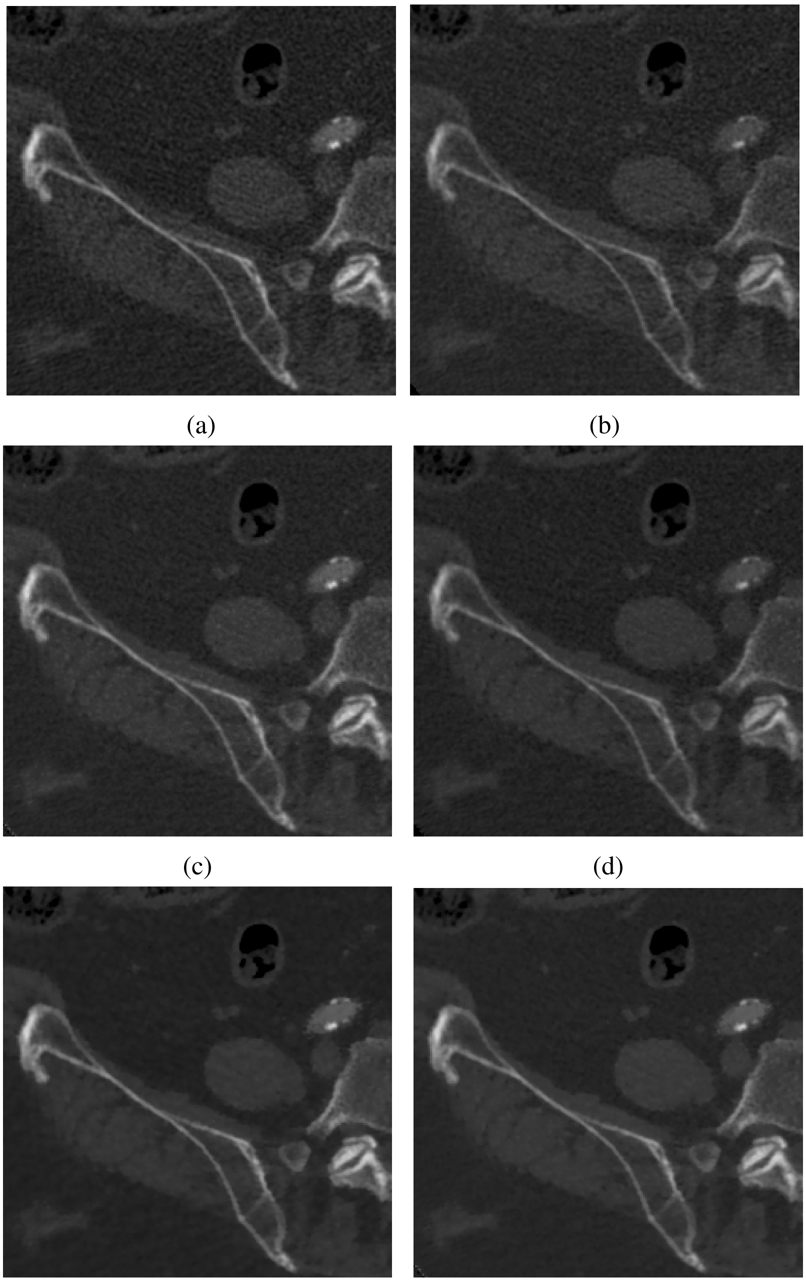

(a) (b)

(c) (d)

(e) (f)

Figure 4.3: Results depicting the entire noise reduction pipeline in the pelvis region. The bilateral filter parameters are $\sigma_s = 1.4$, $\sigma_r = 30$. (a) shows the original low energy image and (b) the original high energy one. (c) presents the KCNR of the low energy image and (d) the KCNR of the high energy image. (e) displays the DECT bilateral filter applied in the original images, whereas (f) shows the result of the DECT bilateral filter applied on the KCNR processed images.

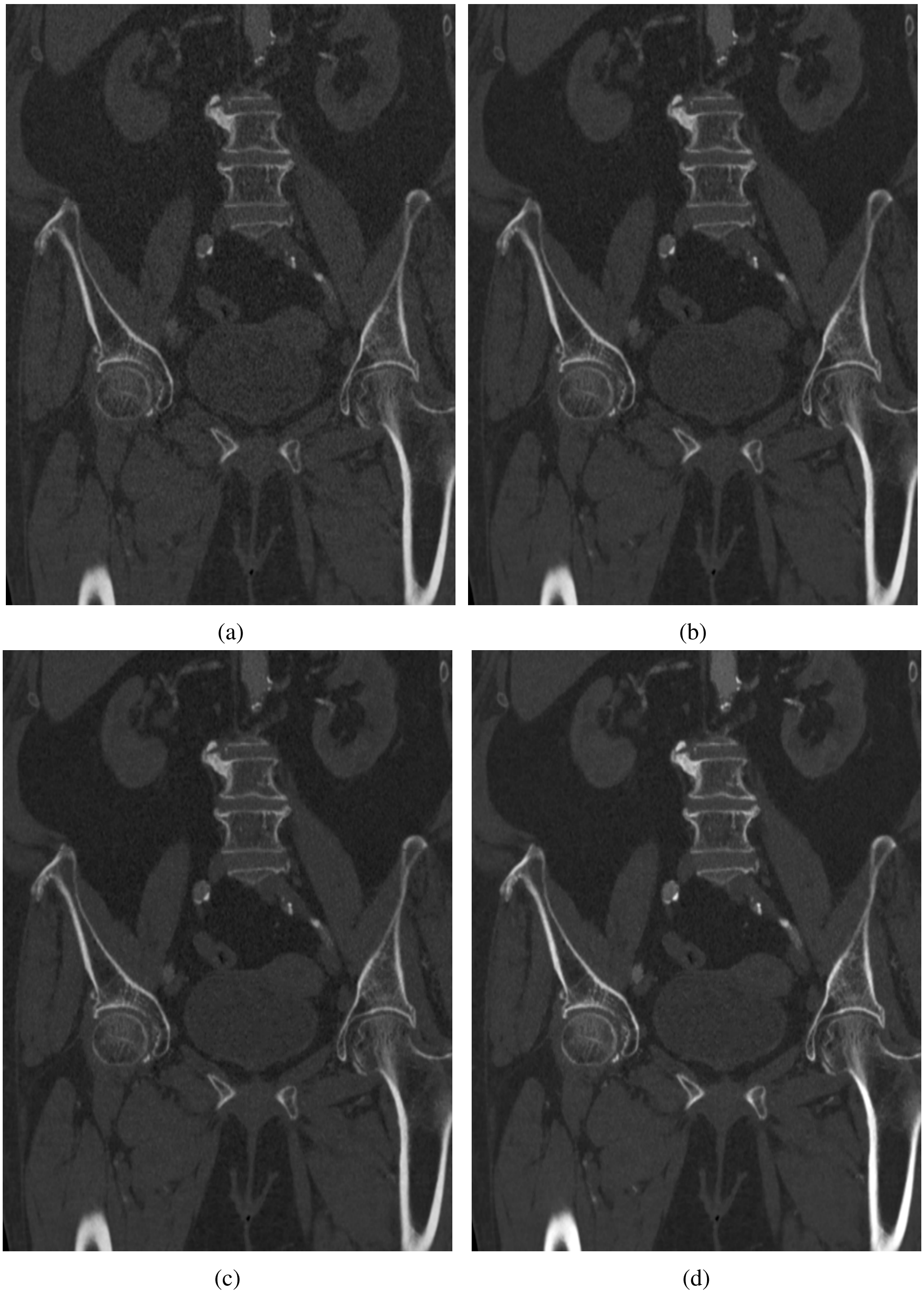

Figure 4.4: Coronal slice images of DECT data set. (a) shows the original high energy image and, (b) the virtual 120kV image. The final result of our pipeline is shown in (c) without the bilateral filter, and in (d) with the bilateral filter using parameters $\sigma_s = 1.5$ and $\sigma_r = 5.0$.

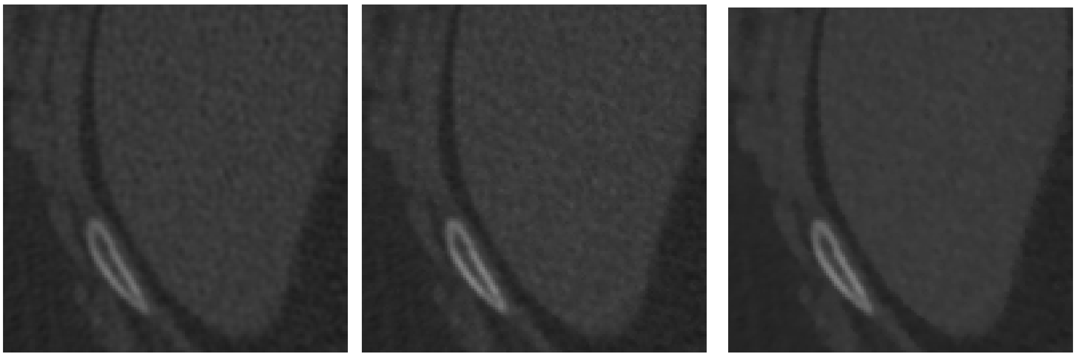

(a) (b) (c)

Figure 4.5: Axial slice images of DECT data set. (a) shows the virtual 120kV image. Final result of our pipeline is shown in (b) without the bilateral filter, and in (c) with the bilateral filter using parameters $\sigma_s = 1.5$ and $\sigma_r = 20.0$.

CHAPTER 5

Conclusion and Future Work

The aim of this work was to get a better understanding of the DECT, to explore additional information provided by the energy dependent imaging and to implement several image enhancing techniques for this specific data. In order to get familiar with the information acquired by DECT it is necessary to obtain knowledge about the attenuation of various materials and its dependance on the energy levels. The spectral information, which lies in the difference between two images obtained at different energy levels, is a valuable tool and we used it effectively in our implemented algorithms. We demonstrated that noise in DECT data sets is correlated and that the KCNR, together with other techniques, can be used to substantially reduce noise. Our algorithms reduce noise without degrading structural information of DECT data sets.

We analyzed common image noise reduction techniques, as well as advanced techniques of noise reduction of DECT data. In order to get the best results from our noise removal pipeline, it is necessary to test and fine tune several parameters, available during the process. For specific anatomical regions of interest different parameter values may be necessary. In general, we demonstrated in this work, that medical DECT data can lead to substantial less noisy data when applying specific algorithms. Nevertheless, a thourough qualitative evaluation has to be done in order to strengthen and justify the results.

As one possible future avenue of our work, we see the application of several segmentation techniques after our noise reduction. An example for such technique would be CT angiography. Some of the implemented noise removal algorithms like the bilateral filter, tend to be very slow when applied to large volumetric data, because our implementation is done on the CPU. Hence, a possible improvement in terms of speed would be to implement a parallel version of the DECT bilateral filter (possibly on the GPU). The Angiovis framework already supports CUDA that provides the functionality of general purpose computing on the GPU. Adopting the noise reduction algorithms in this work to fully utilize CUDA could make our noise reduction pipeline significantly faster.

Bibliography

[1] K.-K. Park, C.-H. Oh, and M. Akay, "Image enhancement by spectral-error correction for dual-energy computed tomography," in *Proceedings of the Annual International Conference of the IEEE on Engineering in Medicine and Biology Society, EMBC*, pp. 8491–8494, 2011.

[2] W. Kalender, E. Klotz, and L. Kostaridou, "An algorithm for noise suppression in dual energy CT material density images," *IEEE Transactions on Medical Imaging*, vol. 7, no. 3, pp. 218–224, 1988.

[3] "Angiovis toolbox." `http://www.angiovis.org/`, Feb. 2014.

[4] Visiongain, "Computed Tomography (CT) Systems: Global Market Outlook 2012-2022." `http://www.visiongain.com/Report/796/Computed-Tomography-%28CT%29-Systems-Global-Market-Outlook-2012-2022`, Feb. 2012.

[5] W. Kalender, *Computertomographie Grundlagen, Gerätetechnologie, Bildqualität, Anwendungen*. Erlangen: Publicis Corp. Publ, 2006.

[6] P. Seidensticker and L. Hofmann, *Dual Source CT Imaging*. Springer, 2008.

[7] D. R. Holmes, J. G. Fletcher, A. Apel, J. E. Huprich, H. Siddiki, D. M. Hough, B. Schmidt, T. G. Flohr, R. Robb, C. McCollough, M. Wittmer, and C. Eusemann, "Evaluation of non-linear blending in dual-energy computed tomography," *European journal of radiology*, vol. 68, no. 3, pp. 409–413, 2008.

[8] D. J. Brenner and E. J. Hall, "Computed Tomography — An Increasing Source of Radiation Exposure," *New England Journal of Medicine*, vol. 357, no. 22, pp. 2277–2284, 2007.

[9] D. T. Schwartz, "Counter-Point: Are We Really Ordering Too Many CT Scans?," *The western journal of emergency medicine*, vol. 9, no. 2, pp. 120–122, 2008.

[10] E. C. Lasser, C. C. Berry, L. B. Talner, L. C. Santini, E. K. Lang, F. H. Gerber, and H. O. Stolberg, "Pretreatment with corticosteroids to alleviate reactions to intravenous contrast material," *New England Journal of Medicine*, vol. 317, no. 14, pp. 845–849, 1987.

[11] H. Wang, H. S. Wang, and Z. P. Liu, "Agents that induce pseudo-allergic reaction," *Drug Discoveries & Therapeutics*, vol. 5, no. 5, pp. 211–219, 2011.

[12] H. S. Thomsen, “Guidelines for contrast media from the European Society of Urogenital Radiology,” *American Journal of Roentgenology*, vol. 181, no. 6, pp. 1463–1471, 2003.

[13] C. H. McCollough, A. N. Primak, O. Saba, H. Bruder, K. Stierstorfer, R. Raupach, C. Suess, B. Schmidt, B. M. Ohnesorge, and T. G. Flohr, “Dose performance of a 64-channel dual-source CT scanner,” *Radiology*, vol. 243, no. 3, pp. 775–784, 2007.

[14] W. Kalender, *Computed Tomography: Fundamentals, System Technology, Image Quality, Applications*. Wiley, 2011.

[15] T. Flohr, C. H. McCollough, H. Bruder, M. Petersilka, K. Gruber, C. Süß, M. Grasruck, K. Stierstorfer, B. Krauss, R. Raupach, A. Primak, A. Küttner, S. Achenbach, C. Becker, A. Kopp, and B. Ohnesorge, “First performance evaluation of a dual-source CT (DSCT) system,” *European Radiology*, vol. 16, no. 6, pp. 1405–1405, 2006.

[16] B. R. Matlaga, S. Kawamoto, and E. Fishman, “Dual source computed tomography: a novel technique to determine stone composition,” *Urology*, vol. 72, no. 5, pp. 1164–1168, 2008.

[17] W. Burger and M. J. Burge, *Digitale Bildverarbeitung : Eine Einführung mit Java und ImageJ*. Berlin, Heidelberg: Springer-Verlag, 2., revised ed., 2005.

[18] R. J. Warp and J. T. Dobbins III, “Quantitative evaluation of noise reduction strategies in dual-energy imaging,” *Medical physics*, vol. 30, no. 2, p. 190, 2003.

[19] K.-K. Park, *A New Approach for the Enhancement of Dual-energy Computed Tomography Images*. PhD thesis, Arizona State University, 2011.

[20] C. Tomasi and R. Manduchi, “Bilateral filtering for gray and color images,” in *Proceedings of the Sixth International Conference on Computer Vision*, pp. 839–846, 1998.

[21] G. Petschnigg, R. Szeliski, M. Agrawala, M. Cohen, H. Hoppe, and K. Toyama, “Digital photography with flash and no-flash image pairs,” *ACM Trans. Graph.*, vol. 23, no. 3, pp. 664–672, 2004.

[22] P. Kornprobst and J. Tumblin, *Bilateral filtering: Theory and applications*. Now Publishers Inc, 2009.